

[O II] as a proxy for star formation in AGN host galaxies: beware of extended emission line regions

Natasha Maddox¹★

¹*ASTRON, the Netherlands Institute for Radio Astronomy, Postbus 2, 7990 AA, Dwingeloo, The Netherlands*

Accepted XXX. Received YYY; in original form ZZZ

ABSTRACT

The [O II] 3726+3728Å emission line doublet is often used to estimate star formation rates within the host galaxies of active galactic nuclei (AGN), as it is known to be strongly excited by star formation, but is only weakly excited in the broad and narrow line regions of AGN. However, within AGN host galaxies, [O II] can also be excited in low-density gas located at appreciable distances from the nucleus, but still ionized by the AGN. These AGN extended emission line regions (EELRs) can contribute significant flux to integrated spectra, even in the presence of luminous AGN. Here, we identify EELRs by the presence of the [Ne V] 3426Å emission line, which, like [O II], is not strongly excited in the inner regions of AGN, but is a prominent emission line in the lower density EELRs. Critically, unlike [O II], [Ne V] is not excited by star formation. Therefore, when strong [Ne V] is present in an AGN spectrum, the flux from the EELR is not negligible, implying the [O II] flux is contaminated by emission from the EELR, and is not a good measure of star formation. After removing objects with EELRs identified by [Ne V], the [O II] flux in the host galaxies of radio-loud AGN is found to be higher than that within radio-quiet AGN, which could either indicate higher star-formation rates, or the presence of moderate-velocity shocks. Being mindful of EELRs for upcoming large-area spectroscopic surveys, particularly those tied to radio continuum surveys, will be important for determining star formation rates in AGN host galaxies.

Key words: surveys–galaxies:star formation–quasars:emission lines–radio continuum:galaxies–ISM:general–line:formation

1 INTRODUCTION

The current star formation rate (SFR) is an important observational metric of a galaxy. It tells us the evolutionary state by indicating whether a galaxy is actively building its stellar mass, or if it is passively ageing. Star formation (SF) can also be triggered by, for example, mergers and/or accretion of gas, thus providing information about a galaxy’s environment. The SF history is a crucial underlying factor in establishing the diversity of galaxies we observe throughout the universe.

There are many observables at a variety of wavelengths that serve as calibrated proxies for the current SF in galaxies. These include optical emission lines such as H α , and continuum flux at ultra-violet, far-infrared and radio wavelengths. A comprehensive comparison of various SF tracers can be found in [Hopkins et al. \(2003\)](#).

The relationship between the flux in the [O II] 3726+3728Å emission line doublet (hereinafter referred to as [O II]) and the SFR has been calibrated by a number of authors (e.g. [Kennicutt 1998](#), [Hopkins et al. 2003](#), and [Kewley, Geller, & Jansen 2004](#)). Although it suffers from dust extinction due to the relatively short emission wavelength, [O II] is very useful for estimating SFRs, as it is a strong, easily identified feature and can be seen in moderate resolution optical spectra out to high ($z < 1.5$) redshifts.

Complicating the measurement of SF in some galaxies is the presence of active galactic nuclei (AGN), as the flux from the AGN outshines the stellar component, at some wavelengths by orders of magnitude. In order to measure SF in AGN host galaxies, we require a quantity whose production is dominated by SF rather than AGN. As shown in the quasar composite of [Vanden Berk et al. \(2001\)](#), [O II] is only weakly excited in the narrow line region (NLR) of AGN, and not at all in the broad line region (BLR). However, it is seen in emission from even moderate levels of

★ E-mail: maddox@astron.nl

star formation. It has therefore been used to estimate the SFR in quasar host galaxies (e.g. [Ho 2005](#), [Kim, Ho, & Im 2006](#), [Kalfountzou et al. 2012](#), [Matsuoka et al. 2015](#), and [Vergani et al. 2017](#)).

1.1 Extended Emission Line Regions

AGN are sometimes seen to ionize gas in the host galaxy beyond the BLR and NLR. While the NLR is typically confined to within <1 kiloparsec (kpc) of the nucleus, extended emission line regions (EELRs)¹ can extend throughout the entire host galaxy, spanning tens of kpcs in some cases (e.g. [Fosbury et al. 1982](#), [Spinrad & Djorgovski 1984](#), [Stockton & MacKenty 1987](#), [Fu & Stockton 2009a](#), [Villar-Martín et al. 2011](#), [Husemann et al. 2013](#), [Liu et al. 2013](#), [Liu et al. 2013](#), [Liu, Zakamska, & Greene 2014](#), [Harrison et al. 2014](#), [Husemann et al. 2014](#)). EELRs are spatially and kinematically distinct from the classic AGN NLRs. The gas within an EELR can show velocity differences of several hundreds, to >1000 km s⁻¹ with respect to the systemic velocity of the galaxy, but also very low velocity dispersion ([Fu & Stockton 2009a](#), [Husemann et al. 2013](#)).

Early studies employing long-slit spectroscopy focused on the EELRs within the host galaxies of bright radio sources ([Spinrad & Djorgovski 1984](#), [Unger et al. 1987](#)), investigating possible triggering mechanisms for the nuclear activity, including mergers with gas-rich galaxies. However, EELRs are also now known to be observed in AGN hosts with no appreciable nuclear radio emission and no indications of recent merger activity (e.g. [Villar-Martín et al. 2011](#), [Husemann et al. 2013](#)).

Integral field unit (IFU) spectrographs with wide spectral range and substantial (tens of arcseconds) fields-of-view have been very useful for studying the kinematics and spatial extent of EELRs. [Fu & Stockton \(2009a\)](#) observed eight galaxies known to have extended emission, covering a wide wavelength range, to investigate EELR clouds on small spatial scales. The ratios of their detected emission lines all indicate AGN as the source of the ionizing flux, rather than star formation. Similarly, [Husemann et al. \(2013\)](#), [Liu et al. \(2013\)](#), [Harrison et al. \(2014\)](#) and [Husemann et al. \(2014\)](#) also use IFU observations to isolate regions throughout AGN host galaxies where the gas has been ionized by the AGN.

Many EELR studies focus on optical emission lines such as [O III] 5008Å and H α . However, for studies with wider wavelength coverage, or observations of objects at higher redshifts, shorter wavelength lines are also visible throughout the EELR, including strong [O II]. The lower density of the interstellar gas, of a few hundred cm⁻³ ([Husemann et al. 2014](#)), with respect to the order of magnitude higher density of the AGN NLR, enables [O II] emission, which has a low critical density, to arise within the EELR ([Villar-Martín et al. 2011](#)). [Fu & Stockton \(2009b\)](#) observed a subset of their EELR galaxies in the infrared (IR), but found no signatures of SF in the hosts, thus confirming the

[O II] flux detected in the IFU spectra should be attributed to the EELR, rather than SF.

As both SF and AGN EELRs independently result in strongly excited [O II] throughout the full extent of galaxies via unrelated mechanisms, we require some diagnostics to distinguish between the different ionizing sources. While emission line ratios can be broadly used to determine the source of the ionizing radiation (i.e. AGN or SF), the most commonly used spectral features, including H α , are shifted out of the optical spectroscopic range by moderate, $z \sim 0.4$, redshifts.

Fortunately, there are specific emission lines which are weak in both the high-density medium surrounding AGN as well as star-forming regions. One such emission line is [Ne V] 3426Å, which, due to its high ionization potential (97 eV, compared to 13.6 eV for [O II], [Lide 2005](#)) is not excited by star formation, but as with [O II], is very weak in AGN spectra ([Vanden Berk et al. 2001](#)). Indeed, for observations of EELRs with spectral coverage of these short wavelengths, [Ne V] is often seen as well (e.g. [Spinrad & Djorgovski 1984](#), [Fu & Stockton 2009a](#)).

Here we investigate the subset of AGN which, in addition to emission lines common in either SF or AGN spectra, also show strong [Ne V] in their spectra, and argue that it indicates the presence of an EELR, or in some cases, extreme shocks. Since EELRs also strongly excite [O II], the [O II] in these objects should not be used as a proxy for SF, since the flux in this emission line is contaminated. In Section 2 we investigate the diagnostic power of emission line ratios in determining the properties of the ionizing radiation, and where objects with detected [Ne V] emission lie in this parameter space. Section 3 is a case study of star formation in SDSS quasar host galaxies. A discussion and conclusions are presented in Section 4. Concordance cosmology with $H_0 = 70$ km s⁻¹ Mpc⁻¹ (thus $h \equiv H_0/[100$ km s⁻¹ Mpc⁻¹] = 0.7), $\Omega_m = 0.3$, $\Omega_\Lambda = 0.7$ is assumed throughout. We use laboratory wavelengths for emission lines, taken from Table 2 in [Vanden Berk et al. \(2001\)](#).

2 EMISSION LINE DIAGNOSTICS

The emission lines we are interested in are the [O II] doublet, and [Ne V] 3426Å (referred to as [Ne V]). We also investigated [Ne III] 3869Å (referred to as [Ne III]) but found it to have less diagnostic power than [Ne V]. Fig. 1 shows the variation in emission strengths of these species in two illustrative spectra of AGN selected by the Sloan Digital Sky Survey (SDSS, [York et al. 2000](#)). The top spectrum is dominated by flux from the AGN, and the unusually strong [O II] indicates additional flux from SF. The bottom spectrum shows [O II], but also has equally prominent [Ne V] shortward of [O II] (and [Ne III] longward), which are not strongly excited within the high density broad or narrow line regions of AGN, or by SF activity.

2.1 BPT classification

Ratios of flux from various emission lines can be used to understand the nature of the ionizing radiation exciting the emission (e.g. [Baldwin, Phillips, & Terlevich 1981](#),

¹ We use the term EELR to describe extended emission beyond the NLR which, based on emission line diagnostics, is shown to be gas ionized by the AGN. We do not use the sometimes quoted alternative term ‘extended narrow line region’ (ENLR), to reinforce the fact that the gas is distinct from the NLR.

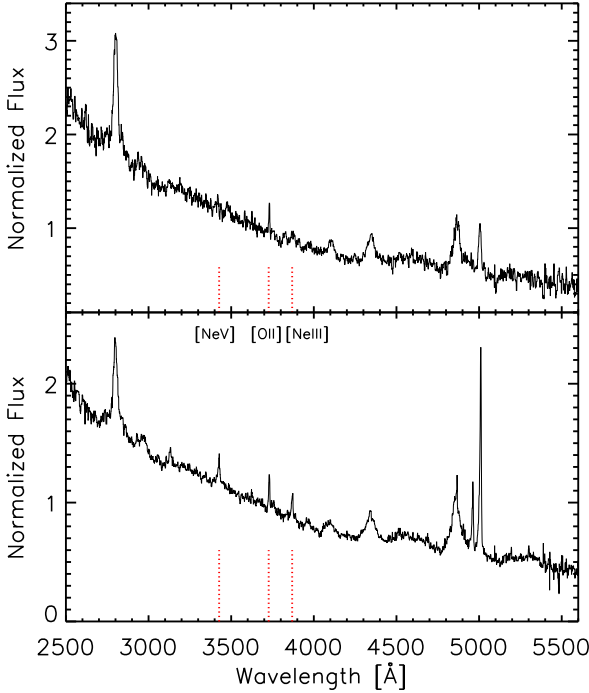


Figure 1. Two SDSS spectra of AGN at $z \sim 0.63$, shifted to the rest-frame, showing the range of [O II] and [Ne V] properties under investigation. The top spectrum has a prominent [O II] emission line but no [Ne V], while the bottom spectrum has strong [O II] emission with similarly strong [Ne V]. [Ne III] is also seen redward of [O II]. The locations of [Ne V], [O II] and [Ne III] are marked along the x-axis with red dotted lines.

Robinson et al. 1987). With specific combinations of spectral features, clear separation between blackbody radiation from stars and radiation with a power-law spectrum is found. The most common of these emission line ratio plots is shown in Fig. 2, often referred to as the ‘BPT diagram’, used here for illustration, where the ratio of [O III] 5008 Å to H β 4862 Å is plotted against [N II] 6585 Å to H α 6564 Å (hereinafter referred to as [O III], H β , [N II] and H α). These two pairs of emission lines are close in wavelength, therefore the ratios are insensitive to dust.

For Fig. 2, we extracted objects from the SDSS database table `emissionLinesPort`, which has measured a large number of spectral features. We use the following lines for investigation: [Ne V]₃₄₂₅, [O II]₃₇₂₆₊₃₇₂₈, [Ne III]₃₈₆₈, H β ₄₈₆₁, [O III]₅₀₀₆, H α ₆₅₆₂ and [N II]₆₅₈₃. We extract only objects within the redshift range of $0.2 < z < 0.25$ to ensure spectral coverage ranging from [Ne V] through [N II]. We imposed no other restrictions on spectral classification or magnitude, but every object is morphologically extended and bright enough to have been selected for spectroscopic follow-up. The resulting population is a mix of galaxies with a range of SFR and AGN of low enough luminosity that the host galaxy is still visible.

Two sequences are immediately seen, separated by the demarcation between AGN and SF as determined by Kauffmann et al. (2003), indicated by the solid blue line in Fig. 2. The less strict demarcation from Kewley et al. (2001) is also shown as a dashed blue line. Objects below and to the

left of the solid line are excited by radiation from SF. The sequence within the SF locus toward lower values of [N II]/H α follows decreasing metallicity (Kewley et al. 2001). Objects lying above and to the right of the dashed line are generally considered to be ionized by radiation consistent with an AGN, with objects that fall between the two lines classified as ‘transition objects’, subjected to a mix of ionization sources.

To illustrate the diagnostic power of [Ne V], and to a lesser extent, [Ne III], to identify EELRs, we highlight the objects with each of these emission lines detected in their spectra. Purple circles mark objects for which [Ne V] is measured at $\geq 5\sigma$. They are almost exclusively within the AGN region, indicating SF is not responsible for exciting this species. Indeed, other works have used the [Ne V] line alone to select samples of AGN from large spectroscopic samples (e.g. Mignoli et al. 2013, Vergani et al. 2017), arguing that it unambiguously indicates the presence of hard ionizing radiation.

There is a small cluster of points at the low-metallicity end of the star formation sequence with detected [Ne V]. The low-metallicity AGN models of Feltre, Charlot, & Gutkin (2016) populate this region of parameter space, for a range of AGN spectral index and ionization parameters. Orange points are objects with $\geq 5\sigma$ [Ne III] emission lines. They are primarily confined to the low-metallicity branch of the SF sequence, but also extend into the AGN cloud. Objects with detected [O II] (not highlighted on this figure) span the full parameter space, as both SF and AGN EELRs excite this species.

Also marked on Fig. 2 as green crosses are points from the IFU observations of EELR clouds from Fu & Stockton (2009a). They all lie within the AGN cloud, and extend toward lower metallicity. Eight of the 20 clouds have measurable [Ne V] emission, but four of the remaining 12 objects do not have spectral coverage shortward of H β , so at least 40 per cent of the Fu & Stockton (2009a) EELR clouds show clear [Ne V].

We conclude that the presence of [Ne V] is a nearly unambiguous indication of an EELR, in agreement with previous work based on [Ne V]-selected AGN, whereas [Ne III] is less reliable, appearing predominantly in objects with BPT emission line ratios indicative of low-metallicity SF. However, the lack of detected [Ne V] emission in \sim half of the Fu & Stockton (2009a) EELR clouds shows that not every EELR shows [Ne V] at the same level as [O II].

2.2 Ionization from shocks

Shocks within the interstellar medium are also capable of exciting a rich spectrum of emission lines. To investigate whether the [O II] and [Ne V] we see in the spectra are due to shocks rather than EELRs, we employ the MAP-PINGS III shock and photoionization modeling code and results from Allen et al. (2008). A comprehensive library of models with varying magnetic field strength, density, metallicity and shock velocity were constructed. The expected fluxes of various species from not only the radiative shock, but also the photoionized precursor medium, along with a combination of the two (shock + precursor, $s+p$), are tabulated. From the models it is clear that a wide variety of shock conditions are capable of exciting [O II], resulting in

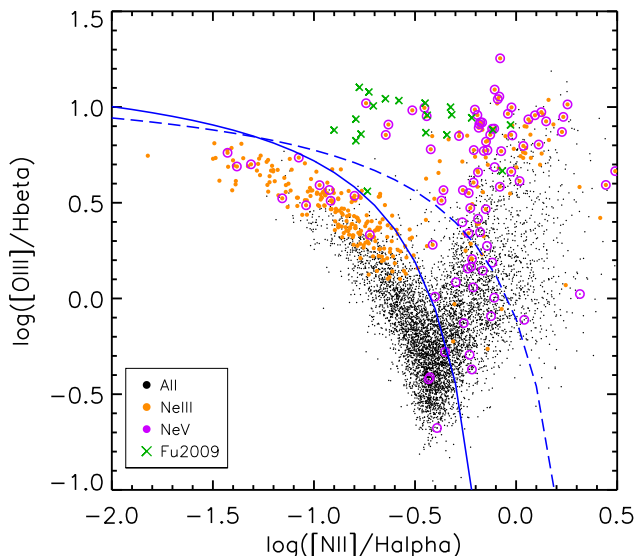


Figure 2. BPT emission line diagnostic diagram for SDSS objects at $0.2 < z < 0.25$ (small black points). The blue solid line is the empirical separation between AGN and SF ionizing radiation, as determined by [Kauffmann et al. \(2003\)](#), while the blue dashed line is the theoretical maximum for SF from [Kewley et al. \(2001\)](#). Points above and to the right of the dashed demarcation line are dominated by AGN-type radiation, while objects between the dashed and solid lines have a mix of ionizing sources. Objects with [Ne III] or [Ne V] additionally detected in their spectra are marked with orange points and purple circles, respectively. The [Ne V] objects lie almost exclusively in the AGN region. Objects with [O II] in their spectra span the full parameter space. The green crosses are the EELR galaxies from [Fu & Stockton \(2009a\)](#).

yet another process that can contribute to this emission line independent of SF.

We focus on combinations of emission line ratios, including [Ne III] and [Ne V], to discriminate between shock and EELR ionization. With respect to the BPT diagram, none of the precursor-only models are found within the AGN cloud for any combination of parameters, so they can be excluded. The models including only the shock does produce AGN-like BPT emission-line ratios, but no appreciable [Ne V] emission. Therefore, only the $s+p$ models are considered further. These are most relevant for observations where the distinct regions are unresolved, as is the case for fibre-based spectroscopy.

All $s+p$ models from the [Allen et al. \(2008\)](#) models except those with SMC-like or LMC-like abundances approximately lie in the AGN region of the BPT diagram. These models also produce [Ne V] at high ($>600 \text{ km s}^{-1}$) shock velocities. However, only at the highest modeled velocities, $\sim 900 \text{ km s}^{-1}$, are the [Ne III]/[Ne V] ratios small, i.e. $\lesssim 5$, typical of the ratios measured in the spectra described in Section 3. Therefore, we find that only the $s+p$ models at the highest velocities are capable of producing emission line ratios consistent with the AGN region of the BPT diagram while also producing [Ne V] and [Ne III] in the correct quantities. The region of the BPT diagram covered by these very specific shocks is restricted to the top right corner of Fig. 2, not spanning the full AGN cloud as shown by the [Ne V]-detected objects. We therefore conclude that while very high

velocity shocks are capable of exciting [Ne V], it is not the dominant mechanism.

The high shock velocities, $\sim 900 \text{ km s}^{-1}$, required to produce [Ne V] imply they are driven by an AGN, and are possibly, but not exclusively, related to radio jets. Therefore, both EELRs and high-velocity shocks result from AGN activity, albeit via different mechanisms. The essential point is that whether via direct photoionization from the AGN or ionization from AGN-driven shocks, the production of [Ne V] is unambiguously related to AGN activity acting on gas beyond the BLR and NLR.

3 CASE STUDY: STAR FORMATION IN AGN HOSTS

Here we revisit the appropriateness of using [O II] to derive the SFR in AGN host galaxies, and investigate the effect of excluding objects which show [Ne V] emission due to EELRs. We restrict our analysis to $0.1 < z < 1.3$, with the lower and upper redshift limits set by requiring coverage of [Ne V] and [O II]. We use the SDSS Data Release 7 (DR7, [Abazajian et al. 2009](#)) quasar catalogue ([Schneider et al. 2010](#)), which has high completeness for quasars at these redshifts. Subsequent data releases focused primarily on higher redshift targets, so DR7 is currently the best dataset for this investigation.

No database tables within SDSS measure our required emission lines for quasars over our full redshift range, so we measure the emission lines ourselves. We have downloaded all the spectra for quasars within the DR7 quasar catalogue at $0.1 < z < 1.3$. We measure [Ne V] and [O II] directly from the spectra, by fitting a Gaussian profile in a spectral window 150 \AA wide centred on the expected line wavelengths. Our measured fluxes and continuum levels for [O II] match very well for objects with measurements in the `galSpecLine` table, which are confined to $z < 0.7$. Note that we fit the combined [O II] doublet with a single Gaussian instead of separating it into two components. Based on visual examination of the resulting fits, and comparison with the SDSS catalogue values, an emission line is considered to be detected if the line is successfully fit automatically, and the equivalent width (EW) is confident if the flux in the line is measured to be $\geq 10^{-16} \text{ erg s}^{-1} \text{ cm}^{-2}$. This flux limit does not result in an effective lower limit on the computed EW, provided the continuum level is sufficiently high.

3.1 [O II] Equivalent widths

Fig. 3 shows the distribution of [O II] EW measured for quasars in the $0.5 < z < 0.6$ redshift bin, converted to the rest-frame. The green vertical line marks the mean of the distribution, which is clearly affected by the small number of objects with high EWs. The green dotted lines show the standard deviation from the mean, which is not strictly meaningful for this type of distribution, but gives an idea of the spread of values. The purple dashed line shows the median of the distribution, which is more robust against the tail toward high EW values. Since it is the high [O II] EW objects that are most often associated with EELRs, we use the mean and standard deviation to parametrize the EW

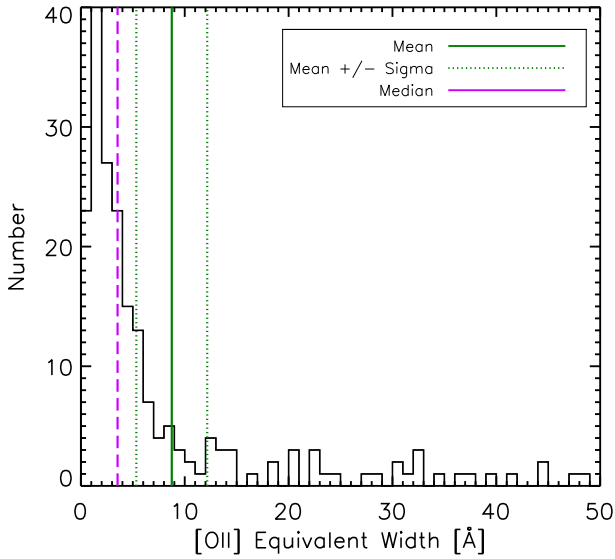


Figure 3. Distribution of equivalent widths of the [O II] emission line for quasars in a single redshift bin. The green solid line is the mean of the distribution, while the purple dashed line is the median. The green dotted lines are the mean \pm the sigma of the distribution.

distributions, with the understanding that the values are illustrative rather than statistically robust.

After measuring the [O II] and [Ne V] emission lines for every spectrum, we divide the quasars into redshift bins of width $\Delta z = 0.1$, and then divide the quasars in each redshift bin into two groups, based on their radio properties. We use the definition from Ivezić et al. (2002) for radio-loudness, R_i , using the Faint Images of the Radio Sky at Twenty-centimeters survey (FIRST, Becker, White, & Helfand 1995) peak flux density provided in the DR7 quasar catalogue. Objects with $R_i > 1$ are classified as radio-loud (RL), while objects with $R_i < 1$ are radio quiet (RQ).

In order to compare the properties of RL and RQ quasars, we create samples matched in redshift and observed i -band magnitude to avoid any biases due to luminosity. For each RL quasar in a redshift bin, we choose the RQ quasar nearest in redshift and magnitude, with matching tolerance of 0.05 in $z - i$ -band magnitude space. We do this both for the full populations, as well as the sub-populations where the [O II] emission line is detected but the [Ne V] emission line is not detected in the individual spectra. From Fig. 1, the full population would include both objects in the figure, whereas the sub-population would only include the object shown in the top panel.

Fig. 4 shows the mean of the derived [O II] EW for the matched samples as a function of redshift, in redshift bins $\Delta z = 0.1$, separated into RL (red) and RQ (blue). When we include all RL and RQ quasars, shown as dotted lines, the RL quasars have much larger [O II] EW than the RQ quasars, to $z = 0.9$. When we exclude objects with detected [Ne V], which imply the [O II] fluxes are contaminated by emission from the EELR, the average EW for RL and RQ are both reduced, and shown as the solid red and blue lines, respectively. The two lines are also much closer, indicating a

smaller difference between the [O II] EW in the RL and RQ populations. Above $z > 0.9$, the RL and RQ subsets have indistinguishable mean [O II] EW, irrespective of the [Ne V] correction. The ‘error bars’ are the illustrative standard deviations, as shown in Fig. 3. A two-sided Kolmogorov-Smirnov (KS) test on the resulting mean EW values for the RL and RQ populations for each redshift bin, shows that the two full populations stop being significantly different at $z = 0.7$, but the uncertainties on the measurements are such that the samples of objects with [Ne V] removed are not formally different at any redshift.

The decrease in [O II] EW in the $0.4 < z < 0.5$ redshift bin for the RL quasars may be a result of the $H\beta$ emission line entering the SDSS i -band. The SDSS quasar catalogue is flux-limited in the i -band, and the prominent $H\beta$ emission line entering the band artificially boosts the apparent magnitude of the objects, resulting in intrinsically less luminous quasars satisfying the flux limit. The fact that the RL quasars are most affected also indicates that the radio properties of the quasar targets also affected their selection, as objects with detections in FIRST are preferentially targeted by the SDSS quasar selection algorithm.

The bottom panel of Fig. 4 shows the fraction of objects with measurable [Ne V] in their spectra, and are thus removed from the sample. At $z < 0.3$, we find the fraction of spectra showing [Ne V] in their spectra is similar for the RL and RQ sub-populations, but at higher redshift, the fraction is higher in RL hosts by 5–15 per cent. The fraction of objects with measurable [Ne V] steadily decreases with increasing redshift, reflecting the fact that at higher redshift, the intrinsically more luminous AGN increasingly dominate the flux in the spectra, with the average luminosity of the objects in the $z = 1$ bin an order of magnitude more luminous than in the $z = 0.1$ bin. At $z \sim 1$, the [Ne V] fractions flatten at around 10 per cent for RQ and 20 per cent for RL. This shows that EELRs (or in addition, strong shocks) are more common within RL quasars, but also visible in a fraction of RQ quasars.

We keep our results as a function of redshift because of the known strong evolution in SFR from $0 < z < 1$, and the increase in intrinsic luminosity of the quasars within the DR7 quasar catalogue. If we average over the entire $0.1 < z < 1.3$ redshift range, we find uncorrected average [O II] EW = 5.8 and 3.4 for RL and RQ quasars, respectively. Removing the [Ne V]-detected objects give corrected mean [O II] EW values of 4.0 and 2.8, for the RL and RQ quasars, respectively. These are smaller than the values quoted in Kalfountzou et al. (2012), who find average [O II] EW for RL and RQ quasars 7.80 and 4.77, respectively. However, note that Kalfountzou et al. (2012) impose a lower limit of EW = 3 to be included in their sample, thus biasing the result to larger values.

3.2 Stacked spectra

We stack the SDSS spectra in bins of redshift of width $\Delta z = 0.1$, using the noise-weighted mean, in order to investigate the mean spectral properties of objects in each redshift bin, along with weak spectral features not identified in individual spectra. We again separate the objects into RL and RQ subsamples. In addition, we create two subsamples for each redshift bin; one containing all objects in the

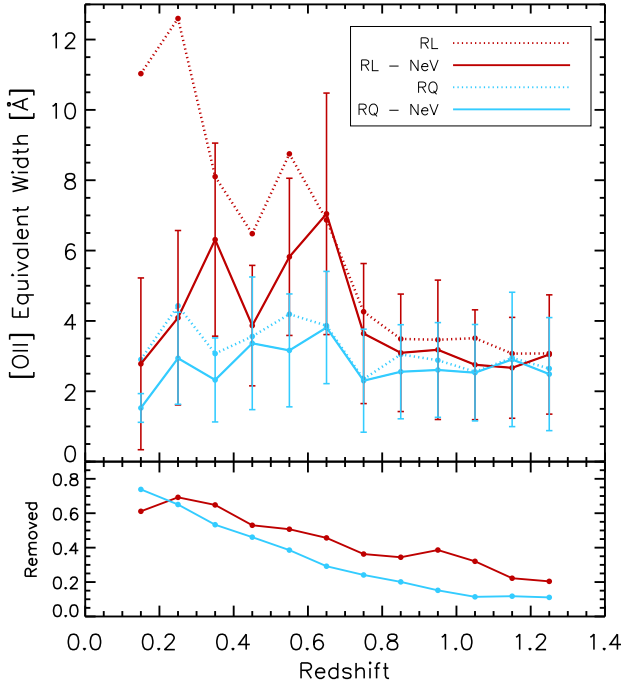


Figure 4. Equivalent width of the [O II] emission line as a function of redshift, for RL (red) and RQ (blue) quasars. The dotted lines are average EW values for each redshift bin, while the solid lines are average EW values for each redshift bin excluding objects with [Ne V] also detected in the spectrum. The lower panel shows the fraction of objects excluded from each bin for having [Ne V] detected in individual spectra.

redshift bin, and one containing only objects where [Ne V] is not detected in individual spectra. This results in four stacked spectra per redshift bin. We then measure the [O II] EW in the stacked spectra. The results are shown in the top panel of Fig. 5. Uncertainties are derived from the uncertainty in placing the continuum level, along with the uncertainty in the fit of the emission line, and are small due to the high signal-to-noise ratio (SNR) of the stacked spectra. The stacked [O II] EW measurements show qualitatively similar behaviour as for the individual spectra in Fig. 4. The high SNR of the stacked spectra enable secure measures of smaller EW values, reaching $\text{EW} \sim 1$ at the highest redshifts probed.

The SDSS composite quasar spectrum from Vanden Berk et al. (2001) shows that the [O II] and [Ne V] emission lines are both intrinsically weak, and at similar flux levels, with the ratio between the two of $[\text{O II}]/[\text{Ne V}] = 1.05$. We investigate the ratio of $[\text{O II}]/[\text{Ne V}]$ in the stacked spectra, as shown in the bottom panel of Fig. 5. Even after excluding quasars with [Ne V] detected in individual spectra, [Ne V] is detected in the higher SNR stacked spectra. The $[\text{O II}]/[\text{Ne V}]$ ratio for RL quasars is ~ 2 , much larger than 1.05, indicating stronger [O II] than would be expected if it was produced by the AGN alone. This corroborates the weak excess seen in Fig. 4, that RL quasar hosts have elevated [O II] with respect to RQ hosts. The RQ hosts have emission line ratios consistent with the ratio from the SDSS quasar composite, indicating the emission

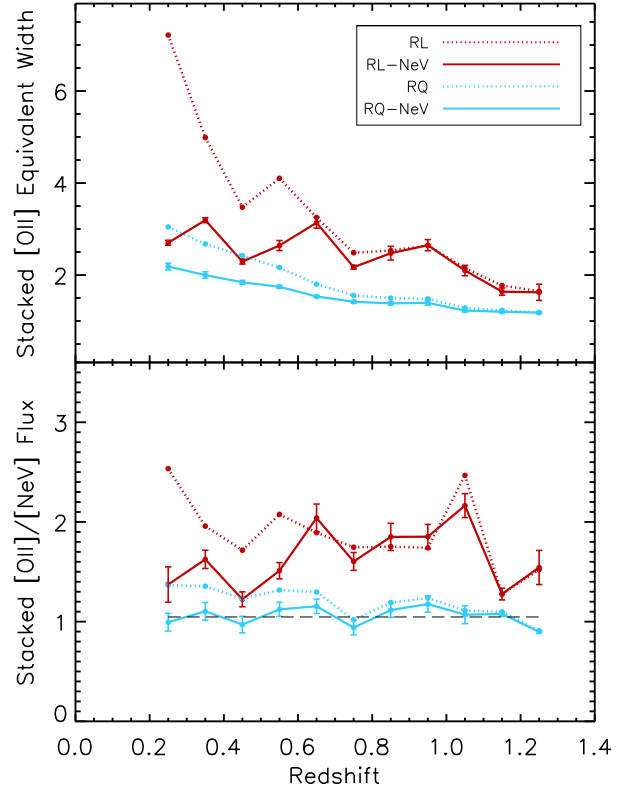


Figure 5. (Top) Equivalent width of the [O II] emission line as a function of redshift, for RL (red) and RQ (blue) quasars. The dotted lines are EW values for the stacked spectrum for each redshift bin including all the spectra, while the solid lines are EW values for the stacked spectrum for each redshift bin excluding objects with [Ne V] also detected in the individual spectra. (Bottom) Ratio of [O II] to [Ne V] fluxes, from the stacked spectra. Also shown as the horizontal black dashed line is the flux ratio of the two emission lines from the SDSS quasar composite spectrum.

lines measured in the stacked spectra are dominated by the AGN NLR.

3.3 Star formation in AGN hosts

The [O II] fluxes from the stacked spectra can be converted into a SFR using the conversion from Kewley, Geller, & Jansen (2004). We use only the stacked spectra that have had objects with [Ne V] visible in individual spectra removed, corresponding to the solid lines in Fig. 5, thus the flux should be free from contamination from EELRs. First, we measure the [O II] flux and directly convert that to a SFR for the RL and RQ subsets, which are shown as red and blue dotted lines in Fig. 6. The SFR values we derive are broadly consistent with those from Matsuoka et al. (2015), who determine SFR of broad-line quasars using [O II] measured from high SNR spectra, with values ranging between $1\text{--}10 M_{\odot} \text{ yr}^{-1}$ over $0 < z < 1$. If we use the [O II] to SFR conversion from Kennicutt (1998) instead of that from Kewley, Geller, & Jansen (2004), the SFRs derived increase slightly, but are still consistent with those from Matsuoka et al. (2015).

However, we know that AGN do indeed produce low

levels of [O II] unrelated to SF, which we must additionally subtract off. We use the intrinsic [O II]/[Ne v] ratio from the SDSS quasar composite, and the [Ne v] measured in the stacked spectra. Recall that individual spectra with [Ne v] visible were not included in the stacks, but due to the resulting high SNR of the stacked spectra, the weak [Ne v] emission line from the AGN NLR is now visible. We assume that the [Ne v] flux in the stacked spectra is the intrinsic flux from the AGN, and not a result of EELRs. From the known intrinsic ratio of [O II]/[Ne v], we can estimate the intrinsic strength of the [O II] line from the AGN NLR and subtract that from the total flux. The remaining corrected [O II] flux is then converted into a SFR as above, and shown on Fig. 6 as the red and blue solid lines.

The doubly-corrected (once to remove contamination from EELRs and once to correct for contribution from the AGN NLR) [O II] flux, when converted into a SFR, results in a SFR for RQ quasars that is consistent with zero. This does not mean that there is no star formation within RQ quasar host galaxies, as we have observed SF within quasar hosts at low redshifts (e.g. Kauffmann et al. 2003), intermediate redshifts (e.g. Matsuoka et al. 2014) and $z > 1$ (e.g. Floyd et al. 2013). It only means that when averaged over many objects within a redshift bin, the SFR is not sufficiently high to produce a strong enough [O II] emission line visible beyond the bright quasar continuum and the flux in the [O II] line naturally produced within the AGN NLR.

In contrast, even after removing contamination from EELRs and the AGN NLR, there is still an excess of [O II] flux seen in the RL quasar hosts. This may be due to either star formation in the host galaxies, or shocks within the host galaxies driven by the radio activity. As we are unable to differentiate between shocks and SF, the solid red line in Fig. 6 is an upper limit to the SFR in the host galaxies of RL quasar hosts.

It is important to note that the primary purpose of this exercise is not to provide a definitive SFR for quasar host galaxies; rather it is intended to show the magnitude of the difference in computed SFRs when accounting for flux within the [O II] emission line that we know does not come from SF.

4 DISCUSSION AND CONCLUSIONS

We have shown that strong [Ne v] emission detected in individual spectra is an indicator of the presence of extended emission excited by an AGN, either via photoionization, or in some extreme cases, via high-velocity AGN-driven shocks. This emission line is not strongly excited within the usual AGN broad or narrow line regions, or by star formation. Table 1 summarizes the relevant sources of ionizing radiation, and whether they excite [O II] and [Ne v]. As [O II] is also excited within EELRs, we conclude that for objects with [Ne v] emission, the [O II] flux is contaminated and cannot be used as a measure of SF.

The fraction of SDSS DR7 quasars removed due to [Ne v] contamination ranges from 70 per cent at low redshift, to 20 per cent and 10 per cent for RL and RQ quasars, respectively, at $z = 1.3$. After removing objects with [Ne v] detected in individual spectra, stacking the remaining spectra reveals a [O II]/[Ne v] flux ratio elevated above that expected from pure AGN emission for the RL quasars, indicating an

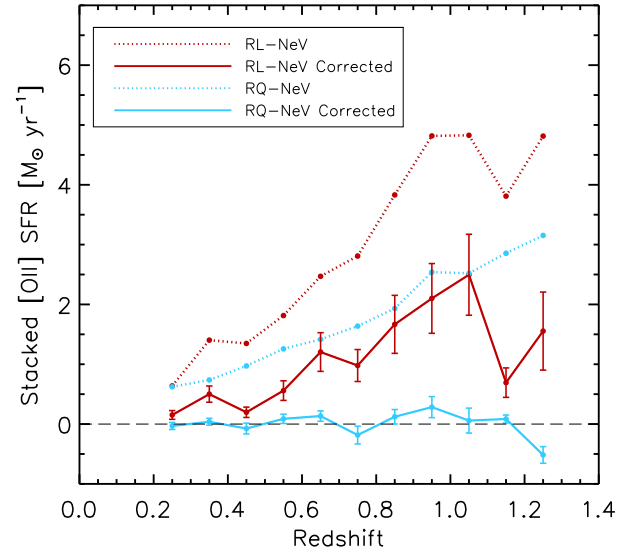


Figure 6. SFR derived from the [O II] flux from the stacked spectra. The dotted lines convert the total measured [O II] flux from each stacked spectrum into a SFR, whereas the solid lines have the [O II] flux intrinsic to the quasar subtracted off. The corrected SFR for RL quasars is non-zero at all redshifts, whereas the corrected SFR for the RQ quasars is consistent with zero.

Table 1. Sources of ionizing radiation within AGN host galaxies, and whether [O II] and [Ne v] are strongly excited by each. * [Ne v] is only excited by shocks at high ($>600\text{km s}^{-1}$) velocities.

Source	[O II]	[Ne v]
SF	Strongly	Weakly
AGN BLR	×	×
AGN NLR	Weakly	Weakly
AGN EELR	Strongly	Strongly
Shocks	Strongly	Strongly*

excess of [O II] emission within these objects. The excess of [O II] flux in RL quasars can be attributed to star formation, but may also be partly due to moderate-velocity shocks from the radio jets acting within the host galaxy, which do not excite [Ne v]. Therefore, the SFRs shown in Fig. 6 are upper limits.

The fact that the EELR diagnostic line [Ne v] is so close to [O II] in wavelength is particularly fortuitous, as they are both visible over the same redshift range, and when taken as a ratio, it does not suffer severely from dust reddening, even though they are in the rest-frame u -band. If there is appreciable amounts of dust in the quasar host galaxies, it will serve to decrease the strengths of both the [O II] and [Ne v]. Therefore, there may be some objects whose [Ne v] has been attenuated below the threshold for detection in individual spectra, in which case these objects were not removed from the stacked samples used for Fig. 5 and Fig. 6 and the [O II] measurements are still contaminated. However, as the SDSS quasars are optically selected, the dust reddening of individual objects is low (Maddox et al. 2012), thus we expect this effect to be small.

A number of large-area radio continuum surveys are

either already underway, or are about to come online. In the Northern hemisphere the Low-Frequency Array (LOFAR, [van Haarlem et al. 2013](#)) is surveying 2π steradians of the northern sky ([Shimwell et al. 2017](#)). Spectroscopy for this survey will be supplied by the new spectrograph to be installed on the William Herschel Telescope (WHT), the WHT Enhanced Area Velocity Explorer (WEAVE, [Dalton et al. 2014](#)), providing redshifts for radio continuum-selected sources ([Smith et al. 2016](#)). Covering the Southern hemisphere, the Evolutionary Map of the Universe (EMU, [Norris et al. 2011](#)) will be undertaken with the Australian SKA Pathfinder (ASKAP, [Johnston et al. 2008](#)). This will be coupled with the spectroscopic redshift survey Taipan ([da Cunha et al. 2017](#)). While the SFR for radio-detected galaxies can be determined directly from the radio flux, computing SFR from $H\alpha$, and to higher redshifts, $[O II]$, will serve as a useful check. In addition, the radio flux can not be used as a SFR indicator for radio-loud quasars, leaving $H\alpha$ and $[O II]$ as the only SF diagnostics available from planned large-area spectroscopic surveys. Other calibrated SF indicators, such as flux at far-infrared (FIR) wavelengths, would require additional observations not currently planned. The importance of understanding and identifying the contribution from EELRs to the $[O II]$ emission line, as measured by the presence of $[Ne V]$, is essential for these projects.

ACKNOWLEDGEMENTS

We thank the anonymous referee for their prompt response and valuable comments which greatly improved this paper. We also acknowledge productive conversations within the AGN group at ASTRON. Funding for the SDSS and SDSS-II has been provided by the Alfred P. Sloan Foundation, the Participating Institutions, the National Science Foundation, the U.S. Department of Energy, the National Aeronautics and Space Administration, the Japanese Monbukagakusho, the Max Planck Society, and the Higher Education Funding Council for England. The SDSS Web Site is <http://www.sdss.org/>.

REFERENCES

- Abazajian K. N., et al., 2009, *ApJS*, 182, 543
 Allen M. G., Groves B. A., Dopita M. A., Sutherland R. S., Kewley L. J., 2008, *ApJS*, 178, 20
 Baldwin J. A., Phillips M. M., Terlevich R., 1981, *PASP*, 93, 5
 Becker R. H., White R. L., Helfand D. J., 1995, *ApJ*, 450, 559
 da Cunha E., et al., 2017, *arXiv*, arXiv:1706.01246
 Dalton G., et al., 2014, *SPIE*, 9147, 91470L
 ultraviolet and optical wavelengths
 Feltre A., Charlot S., Gutkin J., 2016, *MNRAS*, 456, 3354
 Floyd D. J. E., Dunlop J. S., Kukula M. J., Brown M. J. I., McLure R. J., Baum S. A., O’Dea C. P., 2013, *MNRAS*, 429, 2
 Fosbury R. A. E., et al., 1982, *MNRAS*, 201, 991
 Fu H., Stockton A., 2007, *ApJ*, 664, L75
 Fu H., Stockton A., 2008, *ApJ*, 677, 79
 Fu H., Stockton A., 2009a, *ApJ*, 690, 953
 Fu H., Stockton A., 2009b, *ApJ*, 696, 1693
 Harrison C. M., Alexander D. M., Mullaney J. R., Swinbank A. M., 2014, *MNRAS*, 441, 3306
 Ho L. C., 2005, *ApJ*, 629, 680
 Hopkins A. M., et al., 2003, *ApJ*, 599, 971
 Husemann B., Wisotzki L., Sánchez S. F., Jahnke K., 2013, *A&A*, 549, A43
 Husemann B., Jahnke K., Sánchez S. F., Wisotzki L., Nugroho D., Kupko D., Schramm M., 2014, *MNRAS*, 443, 755
 Ivezić Ž., et al., 2002, *AJ*, 124, 2364
 Johnston S., et al., 2008, *ExA*, 22, 151
 Kalfountzou E., Jarvis M. J., Bonfield D. G., Hardcastle M. J., 2012, *MNRAS*, 427, 2401
 Kauffmann G., et al., 2003, *MNRAS*, 346, 1055
 Kennicutt R. C., Jr., 1998, *ARA&A*, 36, 189
 Kewley L. J., Dopita M. A., Sutherland R. S., Heisler C. A., Trevena J., 2001, *ApJ*, 556, 121
 Kewley L. J., Geller M. J., Jansen R. A., 2004, *AJ*, 127, 2002
 Kim M., Ho L. C., Im M., 2006, *ApJ*, 642, 702
 Lide D. R., ed, *CRC Handbook of Chemistry and Physics*, Internet Version 2005, CRC Press, Boca Raton, FL, 2005
 Liu G., Zakamska N. L., Greene J. E., Nesvadba N. P. H., Liu X., 2013, *MNRAS*, 430, 2327
 Liu G., Zakamska N. L., Greene J. E., Nesvadba N. P. H., Liu X., 2013, *MNRAS*, 436, 2576
 Liu G., Zakamska N. L., Greene J. E., 2014, *MNRAS*, 442, 1303
 Maddox N., Hewett P. C., Péroux C., Nestor D. B., Wisotzki L., 2012, *MNRAS*, 424, 2876
 Matsuoka Y., Strauss M. A., Price T. N., III, DiDonato M. S., 2014, *ApJ*, 780, 162
 Matsuoka Y., et al., 2015, *ApJ*, 811, 91
 and optical properties of a $[Ne V]$ -selected sample
 Mignoli M., et al., 2013, *A&A*, 556, A29
 Norris R. P., et al., 2011, *PASA*, 28, 215
 Robinson A., Binette L., Fosbury R. A. E., Tadhunter C. N., 1987, *MNRAS*, 227, 97
 Schneider D. P., et al., 2010, *AJ*, 139, 2360
 Shimwell T. W., et al., 2017, *A&A*, 598, A104
 Smith D. J. B., et al., 2016, *sf2a.conf*, 271
 Spinrad H., Djorgovski S., 1984, *ApJ*, 285, L49
 Stockton A., MacKenty J. W., 1987, *ApJ*, 316, 584
 Unger S. W., Pedlar A., Axon D. J., Whittle M., Meurs E. J. A., Ward M. J., 1987, *MNRAS*, 228, 671
 Vanden Berk D. E., et al., 2001, *AJ*, 122, 549
 van Haarlem M. P., et al., 2013, *A&A*, 556, A2
 Vergani D., et al., 2017, *arXiv*, arXiv:1712.08168
 Villar-Martín M., Tadhunter C., Humphrey A., Encina R. F., Delgado R. G., Torres M. P., Martínez-Sansigre A., 2011, *MNRAS*, 416, 262
 York D. G., et al., 2000, *AJ*, 120, 1579

This paper has been typeset from a \LaTeX file prepared by the author.